THYROID
Volume 26, Number 5, 2016

DOI: 10.1089/thy.2015.0034

Aberrant Cerebellar Development in Mice Lacking Dual Oxidase Maturation Factors

Izuki Amano,[1] Yusuke Takatsuru,[1] Syutaro Toya,[1] Asahi Haijima,[1] Toshiharu Iwasaki,[1] Helmut Grasberger,[2,3] Samuel Refetoff,[2,4,5] and Noriyuki Koibuchi[1]

Background: Thyroid hormone (TH) plays a key role in the developing brain, including the cerebellum. TH deficiency induces organizational changes of the cerebellum, causing cerebellar ataxia. However, the mechanisms causing these abnormalities are poorly understood. Various animal models have been used to study the mechanism. Lacking dual oxidase (DUOX) and its maturation factor (DUOXA) are major inducers of congenital hypothyroidism. Thus, this study examined the organizational changes of the cerebellum using knockout mice of the *Duoxa* gene (*Duoxa–/–*).
Methods: The morphological, behavioral, and electrophysiological changes were analyzed in wild type (*Wt*) and Duoxa-deficient (*Duoxa–/–*) mice from postnatal day (P) 10 to P30. To detect the changes in the expression levels of presynaptic proteins, Western blot analysis was performed.
Results: The proliferation and migration of granule cells was delayed after P15 in *Duoxa–/–* mice. However, these changes disappeared by P25. Although the cerebellar structure of *Duoxa–/–* mice was not significantly different from that of *Wt* mice at P25, motor coordination was impaired. It was also found that the amplitude of paired-pulse facilitation at parallel fiber–Purkinje cell synapses decreased in *Duoxa–/–* mice, particularly at P15. There were no differences between expression levels of presynaptic proteins regulating neurotransmitter release at P25.
Conclusions: These results indicate that the anatomical catch-up growth of the cerebellum did not normalize its function because of the disturbance of neuronal circuits by the combined effect of hypothyroidism and functional disruption of the DUOX/DUOXA complex.

Introduction

Thyroid hormone (TH) is essential for the normal development of the brain (1). TH deficiency during the postnatal period causes congenital hypothyroidism in humans. The typical findings in cretinism are mental retardation, ataxia, and deafness, together with impaired body growth (2,3). TH deficiency in developing rodents induces organizational changes of the cerebellum, causing cerebellar ataxia (4). However, the mechanisms causing this abnormality are poorly understood.

Perinatal hypothyroidism causes various anatomical changes of the rat cerebellum such as reduction of growth and dendritic arborization of Purkinje cells (5,6), reduction of synaptogenesis between Purkinje and granule cells (6,7), delayed myelination (8), and changes in synaptic connections between cerebellar neurons and afferent neuronal fibers (9). These aberrant phenotypes can be rescued only if TH replacement is instituted by postnatal week 2 in rats (5).

Some of the rate-limiting steps of TH synthesis take place at the apical cell membrane of the thyroid follicular cell. To generate hydrogen peroxide (H_2O_2), dual oxidase (DUOX) 2 requires the maturation factor (DUOXA) (10,11). To iodinate thyroglobulin (TG), thyroid peroxidase (TPO) requires H_2O_2 as the final electron acceptor in two steps (12–14). The first step is oxidation of iodide, which is then covalently linked to selected tyrosine residues of TG (12–14). The second step is coupling of two iodotyrosine residues to form iodothyronines (12–14). A defect of DUOX2 or DUOXA2 decreases TH synthesis, causing congenital hypothyroidism in both humans and mice (15–17).

To evaluate the effect of dyshormonogenesis caused by the absence of DUOXA in cerebellar development, the study used *Duoxa* gene knockout mice (*Duoxa–/–*), in which part of both *Duoxa1* and *Duoxa2* exons were deleted (10). *Duoxa+/–* mice were used as dams. Since the TH status of *Duoxa+/–* mice is euthyroid (10), the involvement of an altered maternal TH status on fetal or neonatal development can be

[1]Department of Integrative Physiology, Gunma University Graduate School of Medicine, Maebashi, Japan.
Departments of [2]Medicine, [4]Pediatrics, and [5]Genetics, The University of Chicago, Chicago, Illinois.
[3]Division of Gastroenterology, Department of Internal Medicine, University of Michigan, Ann Arbor, Michigan

excluded. *Duoxa–/–* mice showed delayed disappearance of the external granule cell layer (EGL) followed by a catch-up cerebellar growth, whereas no morphological alteration of Purkinje cells was observed. An electrophysiological study revealed that the amplitude of paired-pulse facilitation at parallel fiber–Purkinje cell synapses decreased at postnatal week 2 but was improved at postnatal week 3. On the other hand, the function of climbing fiber–Purkinje cell synapses was not affected in *Duoxa–/–* mice. Nevertheless, a severe motor coordination defect due to cerebellar ataxia was seen even at postnatal week 3. Daily thyroxine (T4) replacement reversed aberrant growth and motor coordination in *Duoxa–/–* mice. These data indicate that *Duoxa* regulates cerebellar development mainly through the regulation of TH synthesis. It should be noted, however, unlike previous drug-induced congenital hypothyroid models, that alterations of Purkinje cell morphology and electrophysiological properties of climbing fiber–Purkinje cell synapses were not seen. Thus, the cerebellar dysfunction in *Duoxa–/–* mice may be caused by the combined effect of congenital hypothyroidism and functional disruption of the DUOX/DUOXA complex in the brain.

Materials and Methods

All experiments were performed in accordance with the guidelines and protocols approved by the Animal Care and Experimentation Committee, Gunma University. All efforts were made to minimize the suffering and number of animals used in this study.

Animals and treatment

Duoxa–/– mice were generated as described previously (10). Animals were bred in the Animal Facility of Gunma University Graduate School of Medicine. All mice were housed with food and water provided *ad libitum* under controlled temperature (25 ± 5°C), humidity, and illumination (12:12 light–dark cycle; lights on at 7:00 a.m.) conditions. Adult heterozygotes (*Duoxa+/–*) were mated for a suitable reproduction period. Between one and three pups per litter were used in each genotype. Pups from at least three dams were used in each experiment. Some mice received daily subcutaneous injection of 20 μg/kg body weight (BW) levothyroxine (LT4 sodium salt pentahydrate; Sigma, St, Louis, MO) starting at postnatal day (P) 3. This amount is sufficient to correct the hypothyroidism of *Duoxa–/–* mice (18). Pups were weighed and killed at P10, P15, and P25 by decapitation after induction of anesthesia with ketamine/xylazine (22.5 mg/mL ketamine and 1 mg/mL xylazine in 0.9% NaCl, intraperitoneally; 5 mL/kg BW). Their tails were cut to extract DNA to determine their genotype by polymerase chain reaction (PCR) in accordance with the protocol described previously (10). The vermis of the cerebellum was dissected out, rapidly frozen in liquid nitrogen, and stored at –80°C for Western blot analysis. For histological analysis, some brains were fixed in 4% paraformaldehyde in phosphate-buffered saline (PBS) before dissection and cryoprotected in 10%, 20%, and 30% sucrose in PBS (pH 7.4) at 4°C. Cerebella were embedded in the O.C.T. compound (Sakura, Tokyo, Japan), cut at a thickness of 10–20 μm using a cryostat (Microm HM 525; Thermo Scientific, Walthman, MA), and placed on slides for staining with cresyl violet or immunohistochemistry (see below). Tissues were analyzed under a BZ-9000 microscope (Keyence, Osaka, Japan).

Quantitative real-time reverse transcription PCR

Total RNA was extracted at P25 from the cerebellar vermis, cortex, liver, and thyroid using RNeasy (Qiagen, Hilden, Germany). A total of 2 μg of total RNA was used for cDNA synthesis using a High Capacity RNA-to-cDNA kit (Applied Biosystems, Foster City, CA). Specific primers for *Duox1*, *Duox2*, *Duoxa1*, *Duoxa2*, *brain-derived neurotrophic factor* (*Bdnf*), *hairless* (*Hr*), *Krüppel-like factor 9* (*Klf9*), *deiodinase iodothyronine type I* (*Dio1*), *nuclear receptor subfamily 1, group D, member 1* (*Nr1d1*), and *glyceraldehyde 3-phosphate dehydrogenase* (*Gapdh*) as internal controls were used (*Duox1*: Mm01328685_m1; *Duox2*: Mm01326247_m1; *Duoxa1*: Mm01269312_m1; *Duoxa2*: Mm01275445_m1; *Bdnf:* Mm04230607_s1; *Hr*: Mm00498963_m1; *Klf9*: Mm00495172_m1; *Dio1*: Mm00839358_m1; *Nr1d1: Mm00 520708_m1*; and *Gapdh*: Mm99999915_g1; Applied Biosystems). The context sequences for all assays are shown in Supplementary Table S1 (Supplementary Data are available online at www.liebertpub.com/thy). Real-time reverse transcription PCR (RT-PCR) was carried out as described in the instruction manual of the TaqMan Fast Advanced Master mix kit (Applied Biosystems) and the StepOne Real-Time PCR System (Applied Biosystems). The real-time RT-PCR protocol for all genes was 95°C for 20 sec, followed by amplification using 95°C for 1 sec and 60°C for 20 sec (40–80 cycles). Levels of mRNA shown above were normalized by *Gapdh* mRNA level.

Immunohistochemistry

The cerebellar sections were washed with PBS and incubated with 5% normal horse serum in 0.3% Triton X-100 in PBS for 30 min at room temperature. Then, the sections were incubated with a mouse anti-calbindin-D28K antibody (1:3000; Sigma) overnight at 4°C. Next, the sections were incubated with biotinylated horse anti-mouse immunoglobulin G (IgG; 1:200 dilutions) for 45 min. After rinsing in PBS, the sections were incubated with avidin-biotin complex for 1 h and visualized by 3,3′-diaminobenzidine (0.5 mg/mL Tris-HCl containing 0.01% H_2O_2). Sections were then immersed in 0.5% cresyl violet for 1–3 min, dehydrated by graded series of ethanol, cleared in xylene, and placed under coverslips.

Morphometric analysis

Cerebellar areas were measured in cresyl violet-stained midsagittal sections using ImageJ software v1.47 (NIH, Bethesda, MD). All areas of the EGL and molecular layer in one section were measured. Quantitative data were obtained from three sections per mouse, and four mice per genotype and age group were evaluated. The morphology of Purkinje cells was analyzed using midsagittal sections immunostained for calbindin with cresly violet staining. The lengths of the cell body to the first branch point and the sizes of the soma were measured. Quantitative data were obtained from seven to eight cells from one section per mouse, and four mice per genotype were evaluated.

Thyroid function tests

The serum thyrotropin (TSH) concentration was determined by enzyme-linked immunosorbent assay (Rodent Thyroid Stimulating Hormone ELISA test kit ERKR7015; Endocrine Technologies, Inc., Newark, CA). Samples were measured in triplicate. Free T4 (fT4) and free triiodothyronine (fT3) concentrations were measured on a single automated analyzer using the ARCHITECT system (Abbott ARCHITECT i2000; Abbott Laboratories, Maidenhead, United Kingdom). The lowest detectable limits were 0.40 ng/dL and 1.00 pg/mL for fT4 and fT3, respectively. Serum samples from *Duoxa–/–* mice for determining fT4 and fT3 concentrations were collected in one tube from four mice, and five tubes were used for measurement. Twenty *Duoxa–/–mice* from 10 different dams were used for detection of TH status. Sensitivity threshold values were fitted when the concentration was below the sensitivity limits.

Rotarod test

The accelerating rotarod test (model LE8500; Panlab, Barcelona, Spain) was performed at P25 to assess motor coordination. Five rotarod trials with increasing speed from 4 rpm to 40 rpm in 5 min were performed. The time on the rotarod in the last three trials was recorded. Average scores were used for analysis.

Open field test

All mice were tested individually in an open field apparatus at P25. The unit for detecting the motor activity in mice consisted of a 45 cm × 45 cm × 20 cm frame containing a total of 16 × 16 crossed infrared beams at intervals of 2.5 cm, located on the sides (LE 8811; Panlab, S.L.U., Barcelona, Spain). Locomotor activity was assessed on the basis of the analysis of the position and frequency with which the mice crossed the infrared beams. Data were analyzed using the Acti-Track program (Panlab, S.L.U.). Locomotor activity was monitored for 30 min.

Electrophysiology

Experiments were conducted using *Wt* and *Duoxa–/–* mice aged P10–P30. The methods used for the preparation of thin slices and patch-clamp recordings from visually identified Purkinje cells in cerebellar slices were similar to those described previously (19). Briefly, whole-cell patch-clamp recordings of Purkinje cells were performed under an upright microscope (Axioscope; Zeiss, Oberkochen, Germany). The slices were superfused with an external solution containing 120 mM of NaCl, 2.5 mM of KCl, 2 mM of $CaCl_2$, 1 mM of $MgCl_2$, 26 mM of $NaHCO_3$, 1.25 mM of NaH_2PO_4, and 25 mM of glucose, bubbled with 95% O_2 and 5% CO_2. The solution was adjusted to pH 7.4 with HCl and bubbled with 100% O_2. The pipette solution contained 150 mM of Cs gluconate, 8 mM of NaCl, 2 mM of MgATP, 10 mM of HEPES, and 0.1 mM of spermine, and was adjusted to pH 7.2 with gluconic acid. Patch pipettes had resistances of 3–5 MΩ when filled with the pipette solution. Series resistance (5–10 MΩ) was routinely compensated by 70%. To evoke climbing/parallel fiber–excitatory postsynaptic currents (EPSCs) in Purkinje cells, square pulses (0.1 ms, 10–100 μA) were applied through a tungsten concentric bipolar electrode. The signals were filtered at 3 kHz and digitized at 10 kHz for EPSCs. Current responses were recorded with an EPC-8 amplifier (HEKA, Darmstadt, Germany), and a pCLAMP system (v7, Axon Instruments, Foster City, CA) was used for data acquisition and analysis. During ESPC recording, 100 μM of picrotoxin was added to the external solution. All experiments were performed at 30–32°C. The changes in the amplitude and decay time constant (19) of EPSCs in climbing/parallel fiber–Purkinje cell synapses were also examined. The amplitudes of paired-pulse facilitation and depression were calculated using the peak amplitude of each EPSC (20). The decay time constant (τ_w) of ESPCs was calculated as previously reported (19), and 100 nM cyclothiazide (CTZ) was applied to prevent the desensitization of the α-amino-3-hydroxy-5-methylisoxazole-4-propionic acid (AMPA)-type glutamate receptor (21).

Western blot analysis

The dissected cerebella were homogenized in lysis buffer containing 10 mM of Tris-HCl (pH 7.8), 150 mM of NaCl, 1 mM of EDTA, 1% Nonidet P40, and protease inhibitors. The expression levels of postsynaptic membrane proteins (mGluR4, Munc18-1, calmodulin, syntaxin1a, VAMP2, and SNAP25) were extracted from the vermis using a ProteoExtract native membrane protein extraction kit (Calbiochem, San Diego, CA) in accordance with the manufacturer's instruction. The expression levels of proteins were determined by Western blot analysis, as described previously (22,23). Briefly, after boiling for 5 min, protein samples (30 μg) were subjected to 15% SDS-polyacrylamide gel electrophoresis, and separated products were transferred to nitrocellulose membranes. The membranes were blocked with 5% nonfat dry milk in Tris-buffered saline containing 0.1% Tween 20, followed by overnight incubation with the appropriate diluted primary antibodies for mGluR4 (1:1000; Millipore, Billerica, MA), Munc18-1 (1:1000; Cell Signaling, Danvers, MA), calmodulin (1:1000; Cell Signaling), syntaxin1a (1:10000; Abcam, Cambridge, United Kingdom), VAMP2 (1:1000; Cell Signaling), SNAP25 (1:1000; Cell Signaling) and β-actin (1:1000; Cell Signaling). After washing with Tris-buffered saline containing 0.1% Tween 20, the membranes were incubated with a horseradish peroxidase-conjugated anti-rabbit IgG secondary antibody for 1 h at room temperature and detected using an ECL detection system. β-actin was used as a loading control.

Statistical analysis

Statistical comparisons were performed by Student's *t*-test or analyzed by one-, two-, or three-way analysis of variance (ANOVA), followed by the Tukey's test (after one-way ANOVA) or the Bonferroni test (after two- and three-way ANOVA) for *post hoc* analysis. Differences were considered significant at $p < 0.05$. All values are presented as mean ± standard error of the mean. GraphPad Prism v6.0 for Windows (GraphPad Software, San Diego, CA) or SPSS Statistics for Windows v22 (IBM Corp., Armonk, NY) were used for statistical analysis and graphing data.

Results

Growth and TH concentrations

The body weight of *Duoxa–/–* mice during postnatal weeks 2–3 tended to be lower compared with that of *Wt* mice (Table 1). A two-way ANOVA showed significant effects of genotype (male: $F(2, 69) = 39.9$, $p < 0.001$; female: $F(2, 80) = 38.1$, $p < 0.001$) and age (male: $F(2, 69) = 71.0$, $p < 0.001$; female: $F(2, 80) = 51.3$; $p < 0.001$). *Post hoc* analysis by Bonferroni test showed that the body weights of male and female *Duoxa–/–* mice were significantly lower compared with those of *Wt* mice at P25 (male: $t_{20} = 11.5$, $p < 0.001$; female: $t_{27} = 11.2$, $p < 0.001$). The increase in body weight of T4-replaced *Duoxa–/–* mice was similar to that of *Wt* mice. These findings are consistent with those in a previous report (10).

As shown in Table 2, a one-way ANOVA showed no significant differences between three groups for the whole brain weight. However, a one-way ANOVA showed significant differences for the cerebellar weight (male: $F(2, 12) = 21.4$, $p < 0.001$; female: $F(2, 15) = 3.18$; $p < 0.05$). *Post hoc* analysis by Tukey's test indicated that cerebellar weights were significantly lower in *Duoxa–/–* male mice compared with that of *Wt* male mice ($p < 0.01$). Thus, the cerebellum may be more severely affected than other brain regions. Interestingly, T4 replacement could not fully rescue the decrease in cerebellar weight in *Duoxa–/–* mice.

To confirm the presence of hypothyroidism in *Duoxa–/–* mice, serum TSH, fT3, and fT4 concentrations were determined. A one-way ANOVA showed significant differences in TSH and fT4 (TSH: $F(2, 27) = 21.4$, $p < 0.001$; fT4: $F(2, 15) = 6.59$, $p < 0.01$) but not in fT3 ($F(2, 15) = 3.59$, $p = 0.06$). *Post hoc* analysis by Tukey's test showed that *Duoxa–/–* mice had significantly elevated TSH concentrations ($p < 0.001$), indicating that the mice were hypothyroid at P25 (Table 3). The serum fT4 concentration in two of five *Duoxa–/–* groups and the fT3 concentration in all *Duoxa–/–* mice were below the detectable range. On the other hand, no significant differences in hormone levels between *Wt* and T4-replaced mice were observed.

Expression levels of Duox/Duoxa *family*

The expression levels of the *Duox/Duoxa* family members vary among tissues (10). The expression levels of these mRNAs in the cerebellum have not yet been studied. Low expression levels of the *Duox/Duoxa* family mRNAs were found in the *Wt* mice cerebellum compared with those in the thyroid (Supplementary Fig. S1). On the other hand, the expression level of *Duox1* was upregulated in *Duoxa–/–* mice cerebellum, as determined by Student's *t*-test ($p < 0.001$; Supplementary Fig. S1). Thus, the expression pattern of *Duox1* and *Duox2* mRNAs in *Duoxa–/–* mice was different compared with other extrathyroidal tissues such as the colon (10).

Changes of expression levels of TH-responsive genes in Duoxa–/– *mice*

Several TH-responsive genes are expressed in the brain. Among such genes, *Bdnf* plays an important role in cerebellar development (18). *Hr* is also well known as a direct target of TH in brain (24). Both *Bdnf* and *Hr* mRNA expressions were lower in both the cerebellum and the cortex of *Duoxa–/–*

TABLE 1. BODY WEIGHT OF PUPS (G)

	Male			*Female*		
	P10	*P15*	*P25*	*P10*	*P15*	*P25*
Wt	5.0 ± 0.2 (16 litters)	7.1 ± 0.3 (12 litters)	11.3 ± 0.7 (12 litters)	4.9 ± 0.3 (9 litters)	6.6 ± 0.3 (15 litters)	9.2 ± 0.4 (16 litters)
Duoxa–/–	4.3 ± 0.3 (8 litters)	6.3 ± 0.3 (8 litters)	5.5 ± 0.2 (10 litters)***	4.3 ± 0.2 (10 litters)	5.4 ± 0.3 (14 litters)**	5.1 ± 0.2 (13 litters)***
Duoxa–/– + T4	5.3 ± 0.3 (4)	6.4 ± 0.1 (4)	9.4 ± 0.5 (4)	5.2 ± 0.3 (4)	6.4 ± 0.2 (4)	9.4 ± 0.3 (4)

Body weight data are presented as the mean ± standard error of the mean (SEM). The number of litters is shown in parentheses in the *Wt* and *Duoxa–/–* groups. The number of samples is shown in parentheses in the *Duoxa–/–* + T4 group.

**$p < 0.01$; ***$p < 0.001$ by Bonferroni test compared with *Wt* mice (same age).

P, postnatal day; T4, thyroxine.

Table 2. Brain Weight of P25 Mice (mg)

	Male			Female		
	Whole brain	*Cerebellum*	*Percentage of cerebellum/ whole brain*	*Whole brain*	*Cerebellum*	*Percentage of cerebellum/ whole brain*
Wt	384.8 ± 14.3 (7)	46.0 ± 1.0 (7)	12.0 ± 0.5 (7)	382.6 ± 13.5 (9)	45.1 ± 2.2 (9)	11.9 ± 0.6 (9)
Duoxa–/–	397.0 ± 8.8 (4)	38.0 ± 1.0 (4)**	9.6 ± 0.4 (4)*	376.5 ± 2.0 (4)	37.0 ± 2.2 (4)	9.8 ± 0.3 (4)
Duoxa–/– + T4	411.0 ± 6.2 (4)	36.2 ± 1.9 (4)***	8.8 ± 0.4 (4)**	401.3 ± 3.5 (4)	37.5 ± 2.8 (4)	9.3 ± 0.7 (4)

Tissue weight data are presented as the mean ± SEM. The number of samples is shown in parentheses.
*$p < 0.05$; **$p < 0.01$; ***$p < 0.001$ by Tukey's test compared with *Wt* mice (same age).

mice, as determined by Student's *t*-test (cerebellum: *Bdnf* $p < 0.05$, *Hr* $p < 0.001$; cortex: *Bdnf* $p < 0.05$, *Hr* $p < 0.001$; Supplementary Fig. S2). *Dio1*, which converts T4 to T3, is highly expressed in the liver, and its expression is regulated by TH (25,26). The *Dio1* mRNA level in the liver was extremely low in *Duoxa–/–* mice, as determined by Student's *t*-test ($p < 0.05$; Supplementary Fig. S2). On the other hand, the expression levels of *Klf9* and *Nr1d1*, which are also known as a TH-responsive gene, were not significantly changed when evaluated by Student's *t*-test (25,27). These results indicate that *Duoxa–/–* mice are generally hypothyroid in both the brain and the liver. *Klf9* and *Nr1d1* might be regulated by not only TH but also other factors in *Duoxa–/–* mice.

Behavioral analysis

The rotarod test was performed at P25 to examine motor coordination. As shown in Figure 1A, a one-way ANOVA showed significant effects on the duration of remaining on the rotarod (male: $F(2, 19) = 27.9$, $p < 0.001$; female: $F(2, 23) = 34.8$, $p < 0.001$). *Post hoc* analysis by Tukey's test indicated that *Duoxa–/–* mice had a significantly shorter remaining time than *Wt* and T4-replaced *Duoxa–/–* mice ($p < 0.001$; Fig. 1A). The open field test was also performed for 30 min to measure the locomotor activity in a novel environment (Fig. 1B). The activity was not significantly different between three groups, as determined by a one-way ANOVA (male: $F(2, 11) = 1.37$, $p = 0.29$; female: $F(2, 17) = 1.25$, $p = 0.31$).

Cerebellar morphology

In normal mice, the EGL usually disappears by P15. As shown in Figure 2, the EGL persisted at P15 in *Duoxa–/–* mice, indicating delayed proliferation and migration of granule cells. The EGL disappeared by P25 (Fig. 2A and B). The branching of dendrites and the sizes of the somas of Purkinje cells at P15 were not significantly different in *Duoxa–/–* compared to those of *Wt* mice (Fig. 3B; Student's *t*-test, $p = 0.52$). As reported previously, the length of dendrites from the soma to the first branch is shorter in drug-induced hypothyroid mice (18). However, in the present study, the length was not statistically different between *Wt* and *Duoxa–/–* mice (Fig. 3B; Student's *t*-test, $p = 0.32$).

Short-term plasticity of parallel fiber–Purkinje cell synapses

To evaluate the synaptic function in the cerebellum, an electrophysiological study was performed on parallel fiber–Purkinje cell synapses and climbing fiber–Purkinje cell synapses. When a pair of pulses was delivered in close succession, EPSCs evoked by the second pulse tended to increase compared with EPSCs evoked by the first pulse in parallel fiber–Purkinje cell synapses. Such a phenomenon is called paired-pulse facilitation, which reflects presynaptic plasticity (20). As shown in Figure 4B, the paired-pulse facilitation was recorded in both *Wt* and *Duoxa–/–* mice. The ratio of the second response over the first response was lower in *Duoxa–/–* mice than that of *Wt* mice after P14 (Fig. 4D; two-way ANOVA: group × interval between two pulses, $F(5, 252) = 7.99$; $p < 0.001$). Interestingly, significant differences were detected at a short interval between two pulses of 20 msec (Bonferroni test, $t_{43} = 6.69$; $p < 0.001$), 50 msec ($t_{43} = 6.79$; $p < 0.001$), and 100 msec ($t_{42} = 8.48$, $p < 0.001$). These findings indicate that the presynaptic plasticity at parallel fiber–Purkinje cell synapses was altered in *Duoxa–/–* mice.

The plasticity of climbing fiber–Purkinje cell synapses was also examined, which usually show depression by two pulses delivered in close succession (paired-pulse depression). As shown in Figure 5B, traces of EPSCs were not significantly different between *Wt* and *Duoxa–/–* mice. The short-term

Table 3. Thyroid Hormone Status at P25

	TSH (ng/mL)	*fT3 (pg/ml)*	*fT4 (ng/dl)*
Wt	2.56 ± 0.70 (14)	1.51 ± 0.07 (5)	1.14 ± 0.08 (5)
Duoxa–/–	131.6 ± 9.60 (8)***	1 ± 0.00 (5 groups)	0.49 ± 0.03 (5 groups)
Duoxa–/– + T4	1.22 ± 0.55 (8)	2.09 ± 0.37 (8)	2.49 ± 0.53 (8)

Data are presented as the mean ± SEM. The number of samples is shown in parentheses. The lowest detectable limits were 0.40 ng/dL and 1.00 pg/mL for fT4 and fT3, respectively. Serum samples from *Duoxa–/–* mice for determining fT4 and fT3 concentrations were collected in one group from four mice, and five tubes were used for measurement.
***$p < 0.001$ by Tukey's test compared with *Wt* mice.
TSH, thyrotropin; fT3, free triiodothyronine; fT4, free thyroxine.

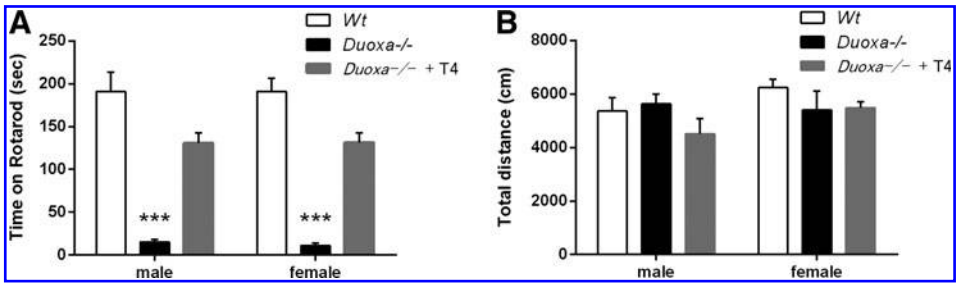

FIG. 1. Behavioral characterization of *Duoxa* knockout mice on P25. (**A**) Duration on accelerating rotarod. *Duoxa–/–* mice (8 male, 7 female) exhibited an impaired performance on the rotarod compared with *Wt* mice (10 male, 15 female) and thyroxine (T4)-replaced *Duoxa–/–* mice (4 male, 4 female). (**B**) Locomotor activities of *Wt* (5 male, 11 female), *Duoxa–/–* (5 male, 5 female), and T4-replaced *Duoxa–/–* (4 male, 4 female) mice in open field test for 30 min. There were no significant differences in traveling distance. Data are presented as mean ± standard error of the mean (SEM). ***$p < 0.001$ determined by Tukey's test compared with *Wt* mice.

plasticity (Fig. 5C; 50 msec interval) and decay time of EPSCs (Fig. 5D) were also not significantly different between the two groups. CTZ, a positive allosteric modulator of AMPA-type glutamate receptors (21), was also applied to reduce the effect of desensitization of these receptors on the decay time constant of EPSCs from climbing fiber–Purkinje cell synapses (21,28). However, the decay time constant was also not significantly different between the two groups (Fig. 5D). These findings indicate that the function of climbing fiber–Purkinje cell synapses was not affected in *Duoxa–/–* mice.

Expression level of presynaptic proteins

Duoxa–/– mice showed attenuated paired-pulse facilitation at parallel fiber–Purkinje cell synapses, indicating alteration of presynaptic function. Thus, the expression levels of presynaptic proteins were examined by Western blot analysis. A large number of proteins are involved in presynaptic function. The presynaptic group III metabotropic glutamate receptor (mGluR) 4 is expressed in the presynaptic active zone and reduces synaptic vesicle release. Munc18-1 and calmodulin are proteins essential for neurotransmission, and they promote soluble NSF attachment protein receptor (SNARE)-mediated vesicle fusion; for a review, see Mochida (29). The expression levels of these representative proteins were examined.

The expression levels of presynaptic proteins were analyzed by a three-way ANOVA (with age, genotype, and sex as factors). A three-way ANOVA of the expression levels of mGluR4, Munc18-1, VAMP2, and SNAP25 showed significant effects of age (mGluR4: $F(2, 31) = 3.61$, $p < 0.05$; Munc18-1: $F(2, 31) = 3.58$, $p < 0.05$; VAMP2: $F(2, 31) = 4.96$, $p < 0.05$; SNAP25: $F(2, 31) = 5.65$, $p < 0.01$). However, there were no differences in calmodulin and Syntaxin1a

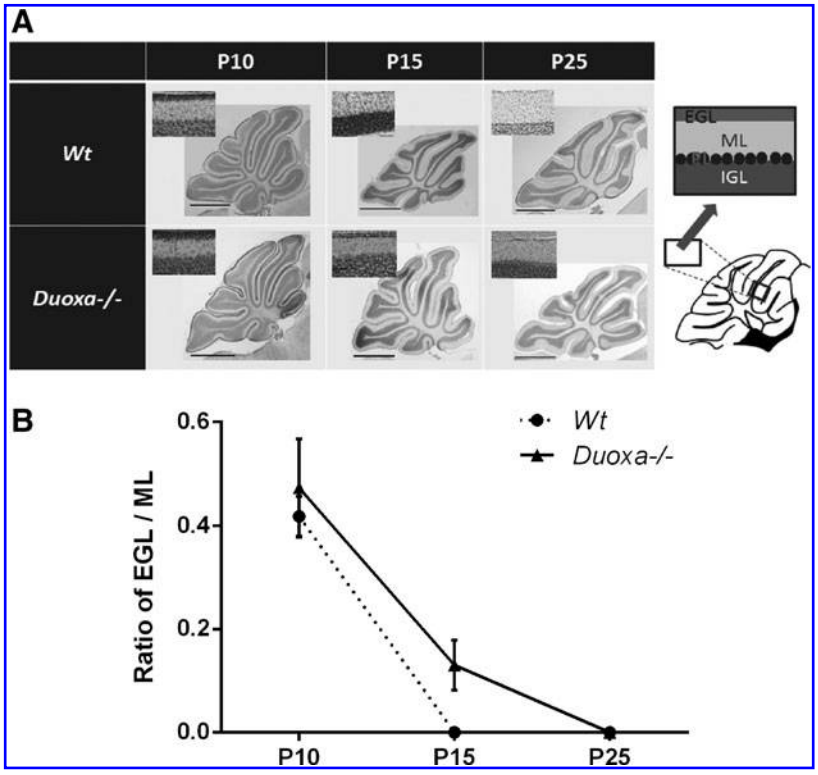

FIG. 2. Morphological alterations of the cerebellum. (**A**) Midsagittal cerebellar sections (vermis) at P10, P15, and P25 stained with cresyl violet. The normal lobulation in the cerebellum is retained. Scale bar: 50 μm (upper left) and 1 mm (middle). (**B**) The ratio of the EGL/ML was measured in all areas of midsagittal sections of the cerebellum. Three sections were analyzed per mouse ($n = 4$). Data are presented as the mean ± SEM. EGL, external granule cell layer; ML, molecular layer; PL, Purkinje cell layer; IGL, internal granule cell layer.

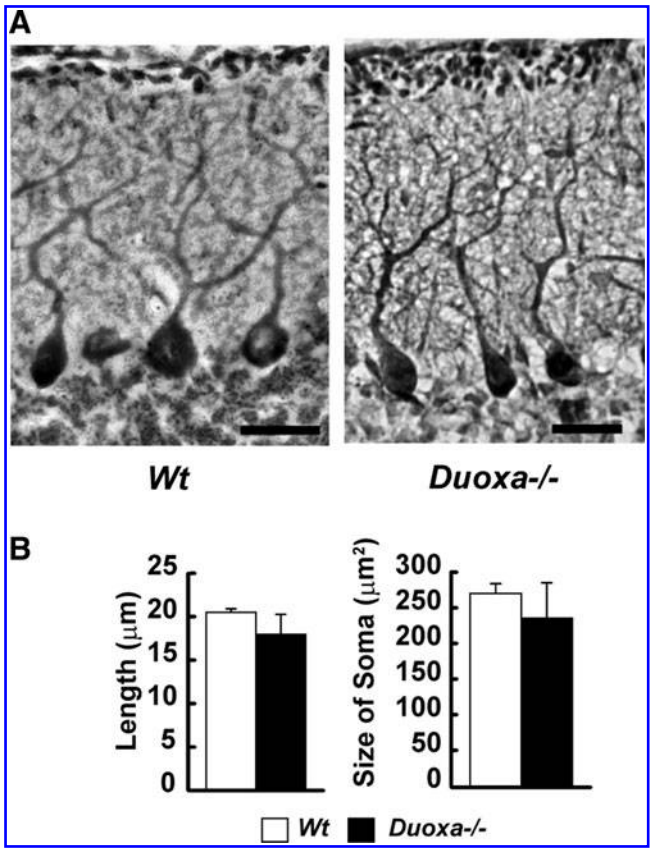

FIG. 3. The morphology of Purkinje cells was not affected by knockout of the *Duoxa* gene. (**A**) Purkinje cells in mid-sagittal sections were stained with cresyl violet and immunostained with calbindin on P15. Scale bar: 100 μm. (**B**) Graph showing the lengths of cell body to the 1st branch point and the sizes of the soma. These values were not statistically different between *Wt* and *Duoxa–/–* mice by Student's *t*-test. Quantitative data were obtained from 30–36 cells from 15–20 sections per mouse, and four mice per genotype were evaluated.

(calmodulin: $F(2, 31) = 0.92$, $p = 0.41$; Syntaxin1a: $F(2, 31) = 1.83$, $p = 0.18$). There were no significant differences by Bonferroni test *post hoc* analysis.

A three-way ANOVA did not show significant effects of sex for the studied proteins, with the exception of SNAP25 (mGluR4: $F(1, 31) = 2.77$, $p = 0.11$; Munc18-1: $F(1, 31) = 3.00$, $p = 0.09$; calmodulin: $F(1, 31) = 0.98$, $p = 0.33$; Syntaxin1a: $F(1, 31) = 0.58$, $p = 0.45$; VAMP2: $F(1, 31) = 2.79$, $p = 0.11$; SNAP25: $F(1, 31) = 15.0$; $p < 0.01$). However, *post hoc* analysis by a Bonferroni test showed no significant differences.

A three-way ANOVA of the expression levels of presynaptic proteins did not show differences between the genotypes (mGluR4: $F(1, 31) = 1.59$, $p = 0.22$; Munc18-1: $F(1, 31) = 1.58$, $p = 0.22$; calmodulin: $F(1, 31) = 0.10$, $p = 0.75$; Syntaxin1a: $F(1, 31) = 0.07$, $p = 0.80$; VAMP2: $F(1, 31) = 1.95$, $p = 0.17$; SNAP25: $F(1, 31)$, $p = 0.93$).

Even though protein expression levels at the presynaptic region of the cerebellum in *Duoxa–/–* mice before P15 was not consistent with the alterations of electrical physiological properties (Figs. 4 and 6), it is concluded that the presynaptic function in the developing cerebellum is impaired in *Duoxa–/–* mice.

Discussion

Duoxa–/– mice showed various morphological changes (e.g., retardation of granule cell migration; Fig. 2). Motor coordination function was also disturbed (Fig. 1) and parallel fiber–Purkinje cell synaptic function (Fig. 4) was altered. Interestingly, the abnormal phenotype in this mouse is not entirely consistent with the findings in other congenital hypothyroid animal models (e.g., Purkinje cell morphology, brain size; Fig. 3 and Table 2). Thus, *Duoxa–/–* mice may be a new animal model to study the combined effect of congenital hypothyroidism and DUOXA functional disruption. However, the effect of DUOX/DUOXA on cerebellar development may be smaller than that of TH because of limited expression of *Duox/Duoxa* in the brain (Supplementary Fig. S1).

Phenotypic characteristics of Duoxa–/– *mice*

The morphogenesis of the rodent cerebellar cortex is completed in the early postnatal period after termination of external granule cell migration, neuronal and glial growth, and synaptogenesis. Multiple factors regulating this process are directly or indirectly regulated by TH. The Purkinje cells receive excitatory inputs from parallel fibers of granule cells and climbing fibers from the inferior olive. Parallel fiber–Purkinje cell synaptic connection is established around P12 during granule cell migration. The climbing fiber–Purkinje cell synaptic connection is established much earlier (around P3) (30). Because of such periodic differences, TH may affect them through different pathways, causing different outcomes. The parallel fibers convey the conditioned stimuli through multi synapses, while the climbing fibers convey the unconditioned stimuli through a single synapse (31). The parallel fiber–Purkinje cell synapse may substantially contribute to cerebellar motor learning (32,33). Thus, the disruption of parallel fiber–Purkinje cell synapses (retardation of granule cell maturation) impairs the motor coordination function in *Duoxa–/–* mice.

To study the effect of TH on cerebellar development, several rodent models have been generated. Mice or rats can be rendered hypothyroid by administering anti-thyroid drugs such as propylthiouracil (PTU) or methylmercaptoimidazole through food or drinking water (5,18). These drugs block TH synthesis by inhibiting TPO, which oxidizes iodide and facilitates the iodination of tyrosine residues on TG (18). When drugs are administered during pregnancy or lactation, the fetus and newborn are rendered hypothyroid. However, such treatment induces hypothyroidism in both pups and dams. Maternal hypothyroidism may alter nursing behavior, which may affect the development of the pups. On the other hand, because *Duoxa+/–* mice are not hypothyroid (10), the effect of altered maternal behavior can be eliminated. In this regard, these mice can be a good model for studying the effects of neonatal hypothyroidism.

Using drug-induced hypothyroid rats, Nicholson and Altman showed a reduced cerebellar weight, a prolonged cell proliferation in the EGL and retarded EGL disappearance, a retarded cell differentiation in the molecular and internal granule cell layers, terminal increases in the numbers of granule cells and astrocytes, and a decrease in those of basket cells (34). Legrand (5) and Clos *et al.* (35) showed a decreased dendritic arborization of Purkinje cells with twofold longer primary dendrites, reduction of growth and branching

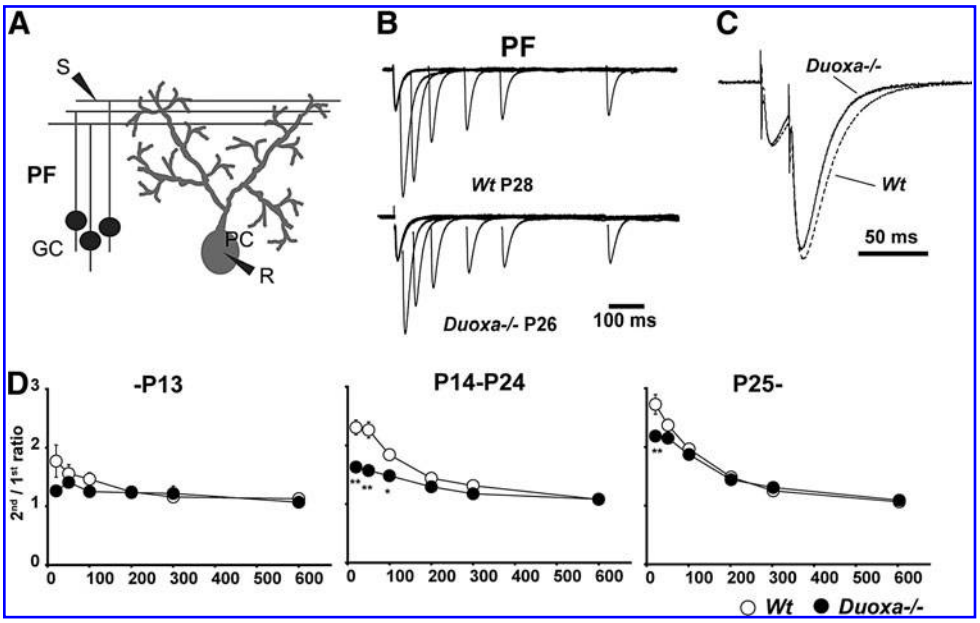

FIG. 4. Paired-pulse facilitation at parallel fiber–Purkinje cell synapses. (**A**) Schema of parallel fiber–Purkinje cell synapse. PC, Purkinje cell; GC, granule cell; R, recording electrode; S, stimulating electrode. (**B**) Representative excitatory postsynaptic current (EPSC) trace of parallel fiber–Purkinje synapses from *Wt* and *Duoxa*–/– mice. The intervals between the first and second stimulations were 20, 50, 100, 200, and 600 ms. (**C**) The traces were normalized by the peak of the first stimulation. The interval between the first and second stimulations was 20 ms. (**D**) Graph showing the ratio of the second peak amplitude divided by the first peak amplitude. The degree of paired-pulse facilitation decreased in *Duoxa*–/– mice after P14 especially at a short interval. The data represent the average of 13 cells in 12 slices from four *Wt* mice (3 male mice) at –P13; 10 cells in 10 slices from three *Duoxa*–/– mice (1 male mouse) at –P13; 25 cells in 20 slices from five *Wt* mice (2 male mice) at P13–P24; 26 cells in 18 slices from four *Duoxa*–/– mice (2 male mice) at P14–P24; 20 cells in 16 slices from five *Wt* mice (2 male mice) at P25–; and 20 cells in 15 slices from four *Duoxa*–/– mice (1 male mouse) at P24–. $*p < 0.05$; $**p < 0.01$ determined by the Bonferroni test.

of dendrites, and shorter parallel fibers with fewer synaptic contacts with Purkinje cells. In *Duoxa*–/– mice, a retardation of the EGL disappearance was also found in this study (Fig. 2). However, the cerebellar catch-up growth motor dysfunction was still detected on the rotarod at P25 when the EGL no longer exists (Fig. 1A), indicating a functional defect of the cerebellum, although an influence of the body weight difference between the control and *Duoxa*–/– mice cannot be excluded.

In the open field test, *Duoxa*–/– mice showed similar travel distances as *Wt* mice (Fig. 1B). In previous studies, using drug-induced hypothyroid or mutant rats, animals tended to

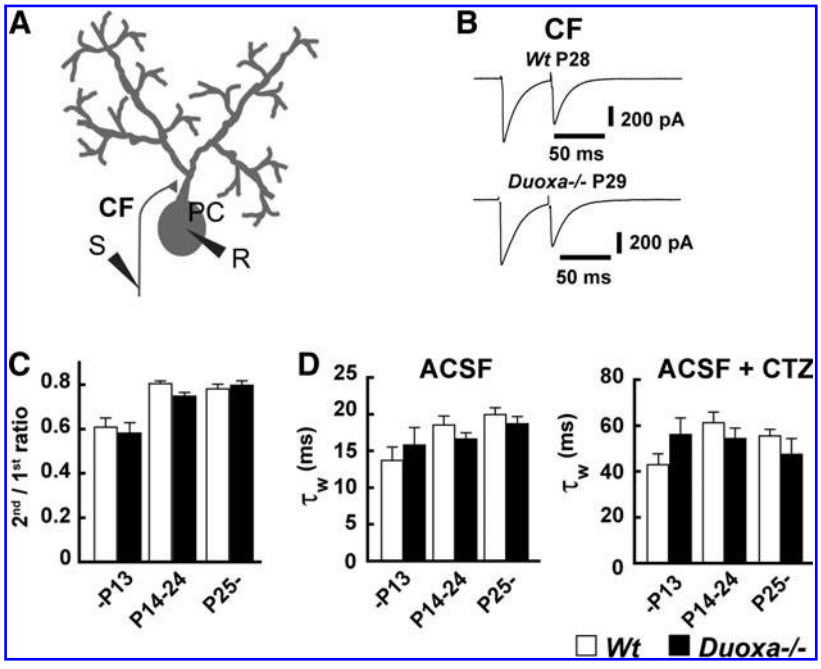

FIG. 5. Paired-pulse depression at climbing fiber–Purkinje cell synapses. (**A**) Schema of climbing fiber–Purkinje cell synapse. (**B**) Representative EPSC trace of climbing fiber–Purkinje cell synapses from *Wt* and *Duoxa*–/– mice. The shape of climbing fiber–Purkinje cell EPSC traces did not show significant differences between *Wt* and *Duoxa*–/– mice. Application of 100 μM cyclothiazide (CTZ) did not cause a significant change either. (**C**) The short-term plasticity was not affected by the knockout of *Duoxa*. (**D**) The decay time constant of EPSCs was not affected under both artificial cerebrospinal fluid (ACSF) condition and CTZ treatment condition. The data are the average of 12 cells in 12 slices from four *Wt* mice (3 male mice) at –P13; 13 cells in 13 slices from three *Duoxa*–/– mice (1 male mouse) at –P13; 20 cells in 20 slices from five *Wt* mice (2 male mice) at P13–P24; 16 cells in 16 slices from four *Duoxa*–/– mice (2 male mice) at P14–P24; 20 cells in 20 slices from five *Wt* mice (2 male mice) at P25–; and 14 cells in 14 slices from four *Duoxa*–/– mice (1 male mouse) at P24–. The Bonferroni test was used in each analysis.

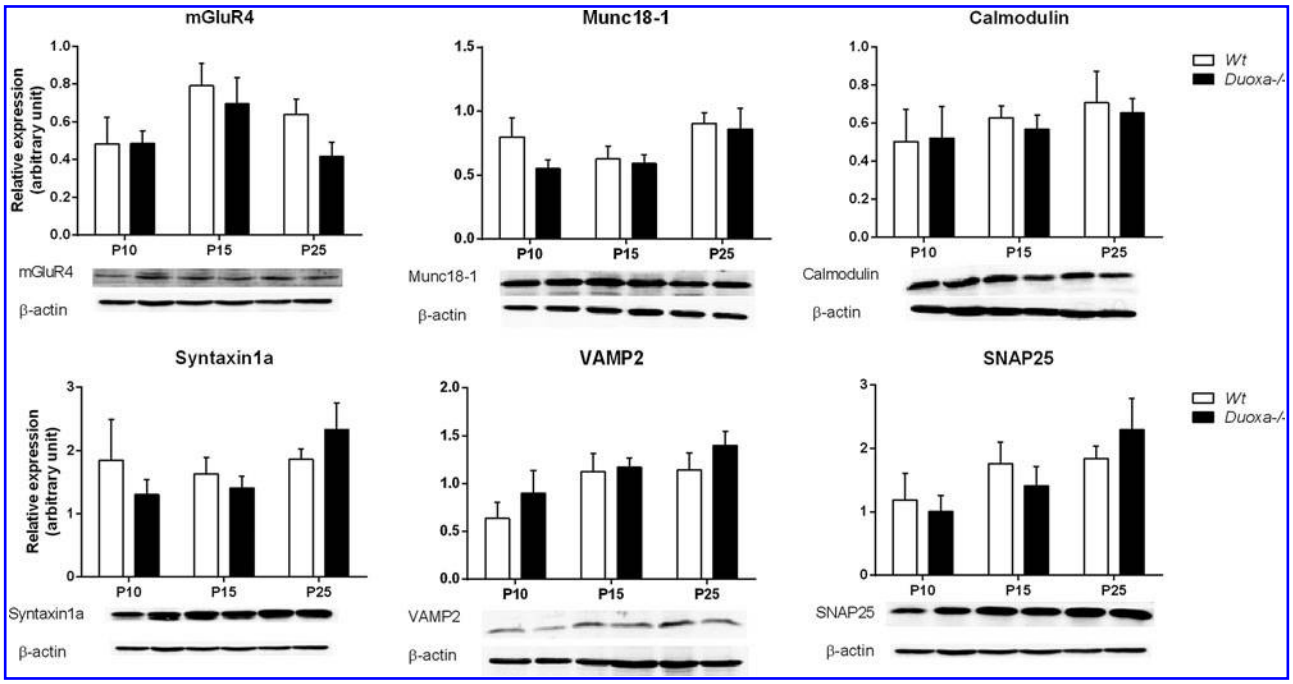

FIG. 6. Western blot analysis of expression levels of mGluR4, Munc18-1, calmodulin, sytaxin1a, VAMP2, and SNAP25 from *Wt* and *Duoxa–/–* mice at P10, P15, and P25 ($n = 6$, sex ratio: 0.5). Images of β-actin are the same as those used for comparison with mGluR4, syntaxin1a, and SNAP25.

be hyperactive in the open field test (36,37). The exact reason causing such differences is not clear. While these differences may be caused by species differences, there is a possibility that the phenotype of *Duoxa–/–* mice may be partly unique compared with those of other hypothyroid animals.

Decrease in neural transmission efficiency in the hypothyroid cerebellum

Parallel fiber–Purkinje cell synapse impairment causes motor coordination and motor learning dysfunctions, which have been studied by electrophysiology (38,39). However, although a motor coordination impairment has also been reported in hypothyroid animals (36,40), electrophysiological analyses have rarely been conducted. Only one study has shown a delay of the evolution of excitations between parallel fibers and Purkinje cells, especially at P10–P20, and a slight disturbance of the climbing fiber responses of Purkinje cells after P9, with recovery by P30 (41). In the present study, the short-term plasticity of parallel fiber–Purkinje cell synapses was affected in *Duoxa–/–* mice (Fig. 4). On the other hand, the short-term plasticity of climbing fiber–Purkinje cell synapses was not affected (Fig. 5). These findings indicate that the release of neurotransmitters at parallel fiber–Purkinje cell synapses is disrupted, whereas the effects on climbing fiber–Purkinje cell synapses are negligible in *Duoxa–/–* mice. This is a unique feature of *Duoxa–/–* mice compared with other rodent hypothyroid models. Although the exact reason for this difference is not clear, *Duoxa–/–* may have a different phenotype compared with other mutants, since no aberrant Purkinje cell morphology was observed (Fig. 3). Further study is required to clarify these points.

To clarify the mechanism underlying the change in electrophysiological properties further, the expression of presynaptic proteins was measured. Proteins measured in the present study play crucial roles in the depression of synaptic transmission (mGluR4) (42–46) and the exocytosis of neurotransmitters (Munc18-1, calmodulin, syntaxin1a, VAMP2, and SNAP25) (29,47–49). The findings indicate that the change in electrophysiological properties is not be caused by an altered expression of these presynaptic proteins, which could cause the disruption of neurotransmitter release. In rats with drug-induced hypothyroidism, on the other hand, the numbers of granule cells and parallel fiber–Purkinje cell synapses are decreased (50–52). Taken together, the decrease in the neural transmission efficiency in *Duoxa–/–* mice is not caused by a change in synaptic property, but by alterations of neuronal circuits (synaptogenesis) between parallel fibers and Purkinje cells.

Possibilities of direct effects of Duox/Duoxa on cerebellar development

In the present and one previous study (10), *Duoxa–/–* mice showed severe hypothyroidism. However, although the phenotype of cerebellar dysfunction in *Duoxa–/–* was similar to those of other congenital hypothyroid animal models, several differences could be observed. For example, the *rdw/rdw* rat, a thyroid dyshormonogenesis animal caused by a mutation in the *Tg* gene, shows not only a severe motor coordination impairment and retarded migration of granule cells, but also small somata and poor dendritic arborization of Purkinje cells (36). In contrast, *Duoxa–/–* mice did not show aberrant Purkinje cell morphology. Furthermore, the short-term plasticity of climbing fiber–Purkinje cell synapses was not affected. Nevertheless, the mice showed a similar motor coordination defect on the rotarod, as did the *rdw/rdw* rats. Such a difference may not only be caused by neonatal hypothyroidism. Rather, DUOX/DUOXA may be directly

involved in brain development. DUOXA1/2 are members of the NADPH oxidase (NOX) protein families and play a critical role in the production of reactive oxygen species (ROS) (53). Coyoy *et al*. identified specific patterns of the expression levels of other members of the family (such as NOX1, NOX2, and NOX4) and ROS generation during various stages of rat cerebellar development (54). Damiano *et al*. reported that DUOX1/2 protein levels were increased by platelet-derived growth factor through production of ROS (55). Based on these findings, one may hypothesize that *Duox/Duoxa* may help the formation and maintenance of synapses in the neuron. However, the physiological functions of the NOX/DUOX family are still unclear (56). In the present study, since we cannot fully explain the mechanism inducing the cerebellar phenotype in *Duoxa-/-* mice, there is a possibility that some phenotypic features may be caused by a direct effect of the functional disruption of the DUOX/DUOXA complex. Further studies are required to clarify the role of NOX/DUOX in brain development.

In conclusion, *Duoxa* deficiency induces developmental hypothyroidism and cerebellar ataxia. Interestingly, although the morphological changes in *Duoxa–/–* mice were negligible compared with mice with PTU-induced hypothyroidism, severe cerebellar dysfunction did persist. These results suggest that the cerebellar dysfunction in *Duoxa–/–* mice may be caused by the combined effect of congenital hypothyroidism and the functional disruption of the DUOX/DUOXA complex in the brain. Thus, *Duoxa–/–* mice may be a unique model to study the role of *Duoxa* on brain development.

Acknowledgments

Serum free T3 and T4 levels were kindly determined by Prof. Masami Murakami, Department of Clinical Laboratory Medicine, Gunma University Graduate School of Medicine. We thank Prof. Hirokazu Hirai, Department of Neurophysiology and Neural Repair, Gunma University Graduate School of Medicine, for permission to use the electrophysiological setup. We thank Mr. Michifumi Kokubo and Ms. Miski Aguhnia Khairinisa, Department of Integrative Physiology, Gunma University Graduate School of Medicine, for technical assistance.

This study was supported by Grant-in-Aid for Scientific Research (B) (25281024) from the Japan Society for the Scientific of Sciences (JSPS) to N.K., by Cosmic Innovative Research Grant from Japan Thyroid Associtation to T.I., and by grant DK 15070 from the National Institutes of Health to S.R.

Author Disclosure Statement

The authors declare that there is no conflict of interest.

References

1. Oppenheimer JH, Schwartz HL 1997 Molecular basis of thyroid hormone-dependent brain development. Endocr Rev **18:**462–475.
2. Rastogi MV, LaFranchi SH 2010 Congenital hypothyroidism. Orphanet J Rare Dis **5:**17.
3. Wiebel J 1976 Cerebellar-ataxic syndrome in children and adolescents with hypothyroidism under treatment. Acta Paediatr Scand **65:**201–205.
4. Koibuchi N, Chin WW 2000 Thyroid hormone action and brain development. Trends Endocrinol Metab **11:**123–128.
5. Legrand J 1967 [Variations, as a function of age, of the response of the cerebellum to the morphogenetic action of the thyroid in rats]. Arch Anat Microsc Morphol Exp **56:**291–307.
6. Nicholson JL, Altman J 1972 The effects of early hypo- and hyperthyroidism on the development of the rat cerebellar cortex. II. Synaptogenesis in the molecular layer. Brain Res **44:**25–36.
7. Nicholson JL, Altman J 1972 Synaptogenesis in the rat cerebellum: effects of early hypo- and hyperthyroidism. Science **176:**530–532.
8. Legrand J 1980 Effects of thyroid hormone on brain development, with particular emphasis on glial cells and myelination. Dev Neurosci 9:279–292.
9. Hajós F, Patel AJ, Balázs R 1973 Effect of thyroid deficiency on the synaptic organization of the rat cerebellar cortex. Brain Res **50:**387–401.
10. Grasberger H, De Deken X, Mayo OB, Raad H, Weiss M, Liao XH, Refetoff S 2012 Mice deficient in dual oxidase maturation factors are severely hypothyroid. Mol Endocrinol **26:**481–492.
11. Grasberger H, Refetoff S 2006 Identification of the maturation factor for dual oxidase. Evolution of an eukaryotic operon equivalent. J Biol Chem **281:**18269–18272.
12. Taurog A, Dorris ML, Lamas L 1974 Comparison of lactoperoxidase- and thyroid peroxidase-catalyzed iodination and coupling. Endocrinology **94:**1286–1294.
13. Taurog A, Dorris ML 1992 Myeloperoxidase-catalyzed iodination and coupling. Arch Biochem Biophys **296:**239–246.
14. Grasberger H 2010 Defects of thyroidal hydrogen peroxide generation in congenital hypothyroidism. Mol Cell Endocrinol **322:**99–106.
15. Moreno JC, Bikker H, Kempers MJ, van Trotsenburg AS, Baas F, de Vijlder JJ, Vulsma T, Ris-Stalpers C 2002 Inactivating mutations in the gene for thyroid oxidase 2 (THOX2) and congenital hypothyroidism. N Engl J Med **347:**95–102.
16. Grasberger H, Refetoff S 2011 Genetic causes of congenital hypothyroidism due to dyshormonogenesis. Curr Opin Pediatr **23:**421–428.
17. Hulur I, Hermanns P, Nestoris C, Heger S, Refetoff S, Pohlenz J, Grasberger H 2011 A single copy of the recently identified dual oxidase maturation factor (DUOXA) 1 gene produces only mild transient hypothyroidism in a patient with a novel biallelic DUOXA2 mutation and monoallelic DUOXA1 deletion. J Clin Endocrinol Metab **96:**E841–845.
18. Koibuchi N, Yamaoka S, Chin WW 2001 Effect of altered thyroid status on neurotrophin gene expression during postnatal development of the mouse cerebellum. Thyroid **11:**205–210.
19. Takatsuru Y, Takayasu Y, Iino M, Nikkuni O, Ueda Y, Tanaka K, Ozawa S 2006 Roles of glial glutamate transporters in shaping EPSCs at the climbing fiber-Purkinje cell synapses. Neurosci Res **54:**140–148.
20. Atluri PP, Regehr WG 1996 Determinants of the time course of facilitation at the granule cell to Purkinje cell synapse. J Neurosci **16:**5661–5671.
21. Takayasu Y, Iino M, Kakegawa W, Maeno H, Watase K, Wada K, Yanagihara D, Miyazaki T, Komine O, Watanabe M, Tanaka K, Ozawa S 2005 Differential roles of glial and neuronal glutamate transporters in Purkinje cell synapses. J Neurosci **25:**8788–8793.

22. Lesmana R, Shimokawa N, Takatsuru Y, Iwasaki T, Koibuchi N 2014 Lactational exposure to hydroxylated polychlorinated biphenyl (OH-PCB 106) causes hyperactivity in male rat pups by aberrant increase in dopamine and its receptor. Environ Toxicol **29:**876–883.
23. Toya S, Takatsuru Y, Kokubo M, Amano I, Shimokawa N, Koibuchi N 2014 Early-life-stress affects the homeostasis of glutamatergic synapses. Eur J Neurosci **40:**3627–3634.
24. Thompson CC 1996 Thyroid hormone-responsive genes in developing cerebellum include a novel synaptotagmin and a hairless homolog. J Neurosci **16:**7832–7840.
25. Ohguchi H, Tanaka T, Uchida A, Magoori K, Kudo H, Kim I, Daigo K, Sakakibara I, Okamura M, Harigae H, Sasaki T, Osborne TF, Gonzalez FJ, Hamakubo T, Kodama T, Sakai J 2008 Hepatocyte nuclear factor 4alpha contributes to thyroid hormone homeostasis by cooperatively regulating the type 1 iodothyronine deiodinase gene with GATA4 and Kruppel-like transcription factor 9. Mol Cell Biol **28:**3917–3931.
26. Ramadoss P, Abraham BJ, Tsai L, Zhou Y, Costa-e-Sousa RH, Ye F, Bilban M, Zhao K, Hollenberg AN 2014 Novel mechanism of positive versus negative regulation by thyroid hormone receptor β1 (TRβ1) identified by genome-wide profiling of binding sites in mouse liver. J Biol Chem **289:**1313–1328.
27. Manzano J, Morte B, Scanlan TS, Bernal J 2003 Differential effects of triiodothyronine and the thyroid hormone receptor beta-specific agonist GC-1 on thyroid hormone target genes in the b ain. Endocrinology **144:**5480–5487.
28. Takayasu Y, Iino M, Ozawa S 2004 Roles of glutamate transporters in shaping excitatory synaptic currents in cerebellar Purkinje cells. Eur J Neurosci **19:**1285–1295.
29. Mochida S 2011 Activity-dependent regulation of synaptic vesicle exocytosis and presynaptic short-term plasticity. Neurosci Res **70:**16–23.
30. Altman J 1972 Postnatal development of the cerebellar cortex in the rat. 3. Maturation of the components of the granular layer. J Comp Neurol **145:**465–513.
31. D'Angelo E 2014 The organization of plasticity in the cerebellar cortex: from synapses to control. Prog Brain Res **210:**31–58.
32. Schonewille M, Belmeguenai A, Koekkoek SK, Houtman SH, Boele HJ, van Beugen BJ, Gao Z, Badura A, Ohtsuki G, Amerika WE, Hosy E, Hoebeek FE, Elgersma Y, Hansel C, De Zeeuw CI 2010 Purkinje cell-specific knockout of the protein phosphatase PP2B impairs potentiation and cerebellar motor learning. Neuron **67:**618–628.
33. van Woerden GM, Hoebeek FE, Gao Z, Nagaraja RY, Hoogenraad CC, Kushner SA, Hansel C, De Zeeuw CI, Elgersma Y 2009 betaCaMKII controls the direction of plasticity at parallel fiber–Purkinje cell synapses. Nat Neurosci **12:**823–825.
34. Nicholson JL, Altman J 1972 The effects of early hypo- and hyperthyroidism on the development of rat cerebellar cortex. I. Cell proliferation and differentiation. Brain Res **44:**13–23.
35. Clos J, Crepel F, Legrand C, Legrand J, Rabie A, Vigouroux E 1974 Thyroid physiology during the postnatal period in the rat: a study of the development of thyroid function and of the morphogenetic effects of thyroxine with special reference to cerebellar maturation. Gen Comp Endocrinol **23:**178–192.
36. Shimokawa N, Yousefi B, Morioka S, Yamaguchi S, Ohsawa A, Hayashi H, Azuma A, Mizuno H, Kasagi M, Masuda H, Jingu H, Furudate SI, Haijima A, Takatsuru Y, Iwasaki T, Umezu M, Koibuchi N 2014 Altered cerebellum development and dopamine distribution in a rat genetic model with congenital hypothyroidism. J Neuroendocrinol **26:**164–175.
37. Negishi T, Kawasaki K, Sekiguchi S, Ishii Y, Kyuwa S, Kuroda Y, Yoshikawa Y 2005 Attention-deficit and hyperactive neurobehavioural characteristics induced by perinatal hypothyroidism in rats. Behav Brain Res **159:**323–331.
38. Kashiwabuchi N, Ikeda K, Araki K, Hirano T, Shibuki K, Takayama C, Inoue Y, Kutsuwada T, Yagi T, Kang Y, et al. 1995 Impairment of motor coordination, Purkinje cell synapse formation, and cerebellar long-term depression in GluR delta 2 mutant mice. Cell **81:**245–252.
39. Hirai H, Pang Z, Bao D, Miyazaki T, Li L, Miura E, Parris J, Rong Y, Watanabe M, Yuzaki M, Morgan JI 2005 Cbln1 is essential for synaptic integrity and plasticity in the cerebellum. Nat Neurosci **8:**1534–1541.
40. Hasebe M, Matsumoto I, Imagawa T, Uehara M 2008 Effects of an anti-thyroid drug, methimazole, administration to rat dams on the cerebellar cortex development in their pups. Int J Dev Neurosci **26:**409–414.
41. Crepel F 1974 Excitatory and inhibitory processes acting upon cerebellar Purkinje cells during maturation in the rat; influence of hypothyroidism. Exp Brain Res **20:**403–420.
42. Kinoshita A, Ohishi H, Nomura S, Shigemoto R, Nakanishi S, Mizuno N 1996 Presynaptic localization of a metabotropic glutamate receptor, mGluR4a, in the cerebellar cortex: a light and electron microscope study in the rat. Neurosci Lett **207:**199–202.
43. Mateos JM, Azkue J, Sarria R, Kuhn R, Grandes P, Knopfel T 1998 Localization of the mGlu4a metabotropic glutamate receptor in rat cerebellar cortex. Histochem Cell Biol **109:**135–139.
44. Mateos JM, Elezgarai I, Benitez R, Osorio A, Bilbao A, Azkue JJ, Kuhn R, Knopfel T, Grandes P 1999 Clustering of the group III metabotropic glutamate receptor 4a at parallel fiber synaptic terminals in the rat cerebellar molecular layer. Neurosci Res **35:**71–74.
45. Corti C, Aldegheri L, Somogyi P, Ferraguti F 2002 Distribution and synaptic localisation of the metabotropic glutamate receptor 4 (mGluR4) in the rodent CNS. Neuroscience **110:**403–420.
46. Pekhletski R, Gerlai R, Overstreet LS, Huang XP, Agopyan N, Slater NT, Abramow-Newerly W, Roder JC, Hampson DR 1996 Impaired cerebellar synaptic plasticity and motor performance in mice lacking the mGluR4 subtype of metabotropic glutamate receptor. J Neurosci **16:**6364–6373.
47. Sudhof TC 2004 The synaptic vesicle cycle. Annu Rev Neurosci **27:**509–547.
48. Rizo J, Sudhof TC 2002 Snares and Munc18 in synaptic vesicle fusion. Nat Rev Neurosci **3:**641–653.
49. Nakajima Y, Mochida S, Okawa K, Nakanishi S 2009 Ca2+-dependent release of Munc18-1 from presynaptic mGluRs in short-term facilitation. Proc Natl Acad Sci U S A **106:**18385–18389.
50. Madeira MD, Paula-Barbosa M, Cadete-Leite A, Tavares MA 1988 Unbiased estimate of cerebellar granule cell numbers in hypothyroid and in sex-age-matched control rats. J Hirnforsch **29:**587–594.
51. Madeira MD, Cadete-Leite A, Andrade JP, Paula-Barbosa MM 1991 Effects of hypothyroidism upon the granular

layer of the dentate gyrus in male and female adult rats: a morphometric study. J Comp Neurol **314:**171–186.
52. Vincent J, Legrand C, Rabie A, Legrand J 1982 Effects of thyroid hormone on synaptogenesis in the molecular layer of the developing rat cerebellum. J Physiol (Paris) **78:**729–738.
53. Dupuy C, Pomerance M, Ohayon R, Noel-Hudson MS, Deme D, Chaaraoui M, Francon J, Virion A 2000 Thyroid oxidase (THOX2) gene expression in the rat thyroid cell line FRTL-5. Biochem Biophys Res Commun **277:**287–292.
54. Coyoy A, Olguin-Albuerne M, Martinez-Briseno P, Moran J 2013 Role of reactive oxygen species and NADPH-oxidase in the development of rat cerebellum. Neurochem Int **62:**998–1011.
55. Damiano S, Fusco R, Morano A, De Mizio M, Paterno R, De Rosa A, Spinelli R, Amente S, Frunzio R, Mondola P, Miot F, Laccetti P, Santillo M, Avvedimento EV 2012 Reactive oxygen species regulate the levels of dual oxidase (Duox1-2) in human neuroblastoma cells. PLoS One **7:**e34405.
56. Nayernia Z, Jaquet V, Krause KH 2014 New insights on NOX enzymes in the central nervous system. Antioxid Redox Signal **20:**2815–2837.

Address correspondence to:
Yusuke Takatsuru, MD, PhD
Department of Integrative Physiology
Gunma University Graduate School of Medicine
Maebashi
Gunma 371-8511
Japan

E-mail: takatsur@gunma-u.ac.jp

This article has been cited by:

1. Michifumi Kokubo, Syutaro Toya, Izuki Amano, Yusuke Takatsuru. 2017. Early-life stress induces motor coordination dysfunction in adult mice. *The Journal of Physiological Sciences* **26**. . [Crossref]
2. Sumbul Jawed Khan, Syeda Nayab Fatima Abidi, Andrea Skinner, Yuan Tian, Rachel K. Smith-Bolton. 2017. The Drosophila Duox maturation factor is a key component of a positive feedback loop that sustains regeneration signaling. *PLOS Genetics* **13**:7, e1006937. [Crossref]
3. Izuki Amano. 2017. Cerebellar Ataxia in Dual Oxidase Maturation Factors (DUOXA) Mutant Mice. *The KITAKANTO Medical Journal* **67**:1, 85-86. [Crossref]
4. Asahi Haijima, Ronny Lesmana, Noriaki Shimokawa, Izuki Amano, Yusuke Takatsuru, Noriyuki Koibuchi. 2017. Differential neurotoxic effects of in utero and lactational exposure to hydroxylated polychlorinated biphenyl (OH-PCB 106) on spontaneous locomotor activity and motor coordination in young adult male mice. *The Journal of Toxicological Sciences* **42**:4, 407-416. [Crossref]
5. Ana P. B. Araujo, Luan P. Diniz, Cristiane M. Eller, Beatriz G. de Matos, Rodrigo Martinez, Flávia C. A. Gomes. 2016. Effects of Transforming Growth Factor Beta 1 in Cerebellar Development: Role in Synapse Formation. *Frontiers in Cellular Neuroscience* **10**. . [Crossref]
6. Noriyuki Koibuchi. Molecular Mechanisms of Thyroid Hormone Synthesis and Secretion 1-9. [Crossref]